Advances in Geological CO_2 Sequestration and Co-Sequestration with O_2

Circe A. Verba*, U.S. DOE National Energy Technology Laboratory & Oregon State University, USA
William K. O'Connor, U.S. DOE National Energy Technology Laboratory
Jason H. Ideker, Assistant Professor & Kearny Faculty Scholar, Oregon State University, USA

Circe Verba is a Ph.D. candidate at Oregon State University & University of Oregon in Geology/Civil Engineering. Her research with the U.S. Department of Energy, National Energy Technology Laboratory addresses the potential of carbon sequestration and cement stability in a CO_2-rich environment.

William O'Connor is a geologist at the U.S. Department of Energy, National Energy Technology Laboratory who studies carbon sequestration by geologic and mineralization methods among other activities. He acquired his MS in Geology & Geophysics from the University of Missouri-Rolla.

Jason H. Ideker is an assistant professor at Oregon State University who studies concrete durability and early-age properties of cement-based material.

ABSTRACT

The injection of CO_2 for Enhanced Oil Recovery (EOR) and sequestration in brine-bearing formations for long term storage has been in practice or under investigation in many locations globally. This study focused on the assessment of cement wellbore seal integrity in CO_2- and CO_2-O_2-saturated brine and supercritical CO_2 environments. Brine chemistries (NaCl, $MgCl_2$, $CaCl_2$) at various saline concentrations were investigated at a pressure of 28.9 MPa (4200 psi) at both 50ºC and 85ºC. These parameters were selected to simulate downhole conditions at several potential CO_2 injection sites in the United States. Class H portland cement is not thermodynamically stable under these conditions and the formation of carbonic acid degrades the cement. Dissociation occurs and leaches cations, forming a $CaCO_3$ buffered zone, amorphous silica, and other secondary minerals. Increased temperature affected the structure of C-S-H and the hydration of the cement leading to higher degradation rates.

Keywords: Carbon sequestration, oil-well cement, oxy-fuel combustion, secondary ettringite formation

INTRODUCTION

The Intergovernmental Panel on Climate Change recommended that mitigation of anthropogenic CO_2 derived from the use of fossil fuels for energy production is necessary. (1). To this end, brine-bearing formations with large potential storage capacity for geologic sequestration of CO_2 have been identified (2,3,4). Candidate formations include enhanced oil recovery reservoirs and pilot tests sites in saline formations under the National Energy Technology Laboratory (NETL) Phase III Regional Partnership programs (5,6). Proposed wellbores use oil-well type portland cements to plug the well and bond the host rock to the steel casing, and are subjected to specific bore depths, high temperature, and high pressure environments (7, 8). In addition, injection of CO_2 into a brine-bearing formation results in the formation of carbonic acid. Portland cement is not thermodynamically stable under these conditions and is subject to dissolution and ionic migration in a CO_2-rich environment. Thus the integrity of the wellbore seal may be compromised, providing a potential leakage pathway up the wellbore into the atmosphere and/or surrounding substrates (9).

CO_2 exists both as a supercritical fluid ($SCCO_2$) and dissolved in CO_2-saturated brines at sequestration injection depth (10). The production of carbonic acid (H_2CO_3) from dissolution of CO_2 into water, heavily alters cement as the portlandite (CH) is dissolved and replaced by $CaCO_{3\ (s)}$, which fills pore spaces (11). Compressive strength increases initially and $CaCO_3$ provides a pH buffer (12). Ongoing diffusion of carbonic acid leaches Ca^{2+} from the cement, creating a zoned alteration rind of amorphous silica. $CaCO_3$ solubility is significantly lower than that of CH so $CaCO_3$ becomes unstable, causing bicarbonate to reach aqueous saturation and local dissolution of calcium species (11, 13). The diffusion of calcium species out of the cement is driven by the fluctuating pH and propagates further degradation. The following equations show the degradation process:

$$CO_2 + H_2O \leftrightarrow H_2CO_3 \leftrightarrow H^+ + HCO_3^- \quad (1)$$

$$HCO_3^- + H^+ \leftrightarrow 2H^+ + CO_3^{2-} \quad (2)$$

$$Ca(OH)_{2(s)} \rightarrow Ca^{2+}{}_{(aq)} + 2OH^-_{(aq)} \quad (3)$$

$$Ca^{2+}{}_{(aq)} + HCO_3^-{}_{(aq)} + OH^-_{(aq)} \rightarrow CaCO_{3(s)} + H_2O \quad (4)$$

$$H_2CO_{3\,(aq)} + C\text{-}S\text{-}H_{(s)} \rightarrow CaCO_{3\,(s)} + H_2O_{(aq)} + am\text{-}SiO_{2(s)} \quad (5)$$

$$H_2CO_{3\,(aq)} + CaCO_{3\,(s)} \rightarrow Ca(HCO3)_{2\,(aq)} \quad (6)$$

The precipitation of salts is encouraged as suggested by Pruess and Müller (14), as injection of CO_2 into the brine increases aqueous phase salinity. Downhole conditions are assumed to

be static due to low formation permeability and porosity, so the CO_2 system and cement reaction can be considered homogeneous (15).

Previous findings suggest that the rates of alteration are low (1 mm to 1 cm [0.04 to 0.4 in] over 30 years) in simple brines (5, 9, 12). It is therefore suggested that CO_2 sequestration is a probable means of carbon storage at those conditions. However, formation brines range in salt species and in salinity, which impact the degree of cement alteration. In the subject study, where salinity was ≤1 *M*, higher CO_2 solubility led to a depth of cement degradation exceeding 1 mm (0.04 in). Where salinity was >1.2 *M*, depth of degradation was ~0.5 mm (0.02 in) after CO_2 exposure of the same duration (16).

Carbon dioxide co-sequestration studies have been limited to SO_2 models (17, 18) and experimental work with CO_2-H_2S, where Fe^{2+} in the C-S-H and iron substitution in ferrite clinker precipitated ettringite and pyrite (19, 20). The interest in co-sequestration is driven by the high cost of CO_2 capture from conventional combustion flue gas, thus novel types of fossil fuel energy conversion systems, such as oxy-fueled combustion, chemical looping combustion, and coal gasification are under investigation. The flue gas from these technologies consists mostly of CO_2 and is therefore ready for sequestration without post-combustion separation. However, excess O_2 and oxidized acid gas species such as SO_2 remain at low concentrations (1-4%) in the untreated combustion flue gas, requiring separation or a co-sequestration methodology. The latter could provide an economic advantage by eliminating the need to remove the O_2 and SO_2 prior to injection. However, these gas species would likely produce a more aggressive environment and potential degradation to cement well seal integrity that is not currently well understood.

RESEARCH SIGNIFICANCE

This research addresses a critical issue in carbon sequestration evaluation and the basic understanding of wellbore cement stability in a CO_2-rich environment. The experimental conditions selected for this study apply to in-situ conditions at potential CO_2 injection sites in the United States. The multiple chloride species and variable concentrations comprising the synthetic brines in this study mark a departure from prior studies. The addition of flue gas co-contaminate gases could provide an economic advantage due to reduced separation costs and potential storage enhancement (physical or mineral trapping). However, the impact of co-sequestration on cement integrity is not clearly understood.

EXPERIMENTAL PROCEDURE

Class H portland (Lafarge, North America) well cement was prepared based on the American Petroleum Institute (API) practices 10B with a w/c of 0.38 (21). The cement powder (weight percent) comprised of approximately 64.5% tricalcium silicate (C_3S); 11.77% dicalcium silicate (C_2S); 13.24% calcium aluminosulfate (C_4AF); no tricalcium aluminate (C_3A); 2.94% MgO; 2.8% SO_4^{2-}; 0.16% total alkali content (Na_2O); 0.62% free lime, and a loss on ignition (LOI) of 0.73. The cement paste was cast into 25 mm diameter x 152 mm (1x6 in) long PVC-pipe forms, cured at temperatures of 50°C and 85°C under a hydraulic pressure of 28.9 MPa (4200 psi), in 1.2 L stainless steel (316 CrNiMo) static autoclave vessels filled with 600 mL of the synthetic brine. After 24 hours, the forms were removed and the cement paste cylinders held at temperature and pressure for the remainder of the 28 day curing period prior to injection.

The cement paste cylinders were in contact with several CO_2-saturated brines to simulate formation brines and depths at three NETL Phase III Regional Partnership injection sites. Discussion of results using the various brines will be presented in a subsequent publication. This paper focuses on the synthetic "control" brine adjusted to a 1 *M* concentration (0.82 *M* NaCl, 0.02 *M* $MgCl_2$, & 0.16 *M* $CaCl_2$) modeled after several NETL sandstone formation brine chemistries (22).

The CO_2 mixed gas exposure tests were performed using two gas mixtures, 1) pure CO_2 and 2) a mixture of 96% CO_2 + 4% O_2. The tests were conducted at geothermal gradients designed to simulate the sequestration environment, including a supercritical CO_2 headspace and CO_2-saturated brine. The two temperatures were investigated to determine the effect of temperature on the cement paste and specifically on C-S-H structure. Following the curing interval, the autoclaves were purged with the CO_2-gas mixture and then maintained at temperature and pressure for exposure intervals up to 84 days (after the initial 28-day cure). Corrosion of the stainless steel autoclaves was observed during conduct of CO_2-O_2 exposure tests, and is discussed later.

ANALYTICAL PROCEDURE

Petrographic analyses were performed with an optical microscope, and an FEI Inspect F Scanning Electron Microscope (SEM) was used to obtain backscattered electron (BSE) images and energy dispersive spectroscopy (EDS) data on polished epoxy-impregnated

mounts. SEM elemental intensities were optimized using a Cu-Kα standard for quantification and measurement of alteration depth, determined by EDS and spot analysis. Alteration in the cement paste was mapped by measuring the distribution of calcium, silicon, and chlorine in 414 samples over a total of 84 sites. Electron microprobe analysis (EMPA) using wavelength-dispersive spectrometry (WDS) with standard errors, and a correction matrix for cement [oxide weight percent concentrations] was utilized for quantification. X-rays diffracted by specific analyzing crystals (TAP: Na, Al, Mg; LPET: Si, Ca, S, Cl; and LIF: Fe, Ti) determine composition by comparison with intensities of known standards [$Ca_{10}(PO_4)_6Cl_2$, MgO, SiO_2, TiO_2, $CaSO_4$ (anhydrite), Fe_3O_4 (magnetite), and $Na_3KAl_4Si_4O_{16}$ (nepheline)] to the unknown materials in the cement paste. Analysis of cements is very difficult due to the composition of hydrated phases and its intrinsic heterogeneity. Atomic number, adsorption, and fluorescence (ZAF), time dependent intensity (TDI), background continuum, and oxide corrections provide a summation of concentrations representative to the stoichiometric analysis of calcium silicate grains, hydration products, and within alteration zones.

The cementitious phases were identified using X-ray diffraction (XRD) collected by a Rigaku Ultima III with a 40KV/40mA Cu k-α source and a step speed of 1°/min over a scan angle, 185°-90° 2θ. The qualitative analysis of XRD data was performed using the International Center for Diffraction Data (ICDD) pattern databases and Jade Plus software v9.1.4 (23).

Solid chemistry on hydrated paste (ground into powder and vacuum sealed) was determined by several methodologies, including a LECO gas analyzer for sulfur and carbon, lithium meta-borate fusion with X-ray fluorescence (XRF) for metal oxides, carbonate leach and gravimetric analysis for SO_4, CO_2 by coulometer, and acid digestion and titration for FeO. Solution alkalinity was determined by titration, using sodium carbonate and hydrochloric acid. Nitric acid digestion with inductively coupled argon plasma spectroscopy (ICP-AES) methods were used for metals analysis, while ion chromatography was used for Br, Cl, and SO_4.

EXPERIMENTAL RESULTS AND DISCUSSION

Results from pure CO_2 exposure tests (16) were compared to the CO_2-O_2 experimental results, each using the same raw cement batch composition, brine chemistries, and experimental conditions. This methodology isolated the change in conditions to the addition of 4% O_2 to the gas mixture, thus any change in mineralogy, alteration depth as indicated by

$CaCO_3$ and Ca^{2+} depletion, and stainless steel corrosion can be attributed primarily to the O_2 addition.

Pure CO_2 and CO_2-O_2 Gas Injection: Microanalysis of Cement Specimens

Verba et al. (16) found that exposure of Class H cement to pure CO_2 at 50°C and 28.9 MPa (4200 psi), in higher salinity brines of 1-2 *M* NaCl, $MgCl_2$, and $CaCl_2$, resulted in alteration zones in the cement that increase in depth and become more defined with time. The carbonation depths versus time are provided in Table 1, while the alteration zones are depicted in Fig. 1a. Total alteration depth extended into the core up to 1254±441 µm (0.049 in) after an 84-day exposure period. Alteration included large hydration halos surrounding C_2S and C_3S grains as continuous hydration allowed for conversion into interstitial CH and C-S-H. Remnant calcium silicates and hydration products were in the Ca^{2+} depletion zone whereas all calcium silicates in the carbonated zone turned into amorphous silica with a banded appearance from zoning loss of Ca^{2+}. SEM-EDS and EMPA confirmed a Cl-enriched (~3 wt%) and S-enriched zone (1-3 wt%) in the Ca^{2+} depletion zone, presumably incorporated into the C-S-H structure. EMPA identified both Fe^{3+} (at <5%) and Fe^{2+} (<2%) in the C-S-H structure as well.

The higher salinity and multiple chloride species in the brine led to precipitation of large (50-1200 µm; 0.047 in) CH crystals on the exterior of the cement cylinder. Small cubic halite grains (1-15 µm) also crystallized in the cement while the cement maintained a lower pH (<6) and was dehydrated in the presence of early $SCCO_2$. The precipitation of the additional minerals, specifically exterior CH, reduced the maximum alteration depth and permeability after an exposure of 84 days.

CO_2-O_2 (96% CO_2 + 4% O_2) exposures led to more rapid cement degradation and ionic migration behavior compared to the pure CO_2 studies (Fig. 1b,c). The cement cylinders displayed a banded Si-porous zone of remnant silicates, a $CaCO_3$ band with thickness dependent on temperature, and a Ca^{2+} depleted zone. EMPA analyses found that the C-S-H structure contained roughly 1.5 wt% Fe^{2+} and had 20-30% water bound unaltered C-S-H. Significant differences from the pure CO_2 studies included: 1) the transformation of calcium silicates (C_2S) with bordering ferrite grains into polymorphs with significant twinning and 5-10% less Ca^{2+}; 2) precipitation of dendritic hydrotalcite [$Mg_6Al_2(CO_3)(OH)_{16}{\cdot}4H_2O$] on C_4AF grains; and 3) the precipitation of 10-50 µm long ettringite [$Ca_6Al_2(SO_4)_3(OH)_{12}{\cdot}$

1

126H_2O] needles within pores specifically in Ca^{2+} depleted zones (Fig. 2). The authors suggest 2that change in pH between the solution and the cement within the Ca depletion zone allowed 3for ettringite formation, coupled with leaching of Ca^{2+} and Al^{3+}, as well as S previously bound 4in C-S-H.

5

6Ettringite formation occurred after the primary curing stage and during the CO_2-O_2 gas 7exposure interval, after carbonation had occurred as determined by SEM and XRD analysis. 8This secondary [delayed] ettringite formation (DEF) can lead to loss of cement paste 9integrity, degradation, expansion, and fracturing (13). Expansion of the cement paste or the 10development of microfractures could serve as potential leakage pathways for the injected 11gases or liquids, either out of the wellbore or to the wellbore steel casing. Microfractures 12ranging from 0.5-3 µm wide extend from many of the pores containing ettringite, and 13propagated in the least resistant pathway around mineral grains. These are not interpreted as 14an artifact of sample prep, due to the small fracture sizes, where fractures induced during 15sample prep often cut across mineral grains and stem into larger fractures. Etched and pitted 16features were also observed on the silicates and C_4AF, evidence of acid attack. EMPA data 17suggests <2% of the carbonate band contained $FeCO_3$, which could not be confirmed via 18other instrument analyses in such trace amounts.

19

20Total alteration depth versus time of the CO_2-O_2 exposure samples is listed in Table 1. At both 21temperatures, the alteration depth exceeded initial depths (28-days) in comparison to 22pure-CO_2 exposure, but displayed diffuse and nonuniform alteration as shown in Fig. 3. The 2385ºC sample showed the highest rate of degradation with a large, thicker initial $CaCO_3$ band 24compared to pure CO_2 exposure. At 28 days of exposure, the alteration depth was minimal, 25up to 253±59 µm (0.01 in). After 53 days, the alteration zone extended to a depth of 916±94 26µm (0.036 in), and the Ca^{2+} depleted zone ranged from ~0.5- 1 mm (0.02-0.04 in), with large 27pores up to 160 µm (0.0063 in) in diameter. After 73 days, pieces of the cement shed off from 28the cylinder exterior, and alteration exceeded 1-2 mm (0.04-0.08 in). Thus, degradation 29increased in the higher temperature static conditions from 53-73 days of exposure. The 50ºC 30sample, on the other hand, displayed an alteration depth at 514±109 µm (0.02 in) after 28 31days, exceeded 680±132 µm (0.027in) after 56 days, but remained fairly constant over the 32duration of the test exposure.

33

1

1Solid and Solution Chemistry

2Solid chemistry of the unhydrated portland Class H cement, hydrated cement paste and 3post-gas exposure cement samples are included in Table 2. Brine solution chemistry for the 4post-curing interval and post gas-exposure intervals is included in Table 3.

5

6The product solids from the pure-CO_2 tests showed a slight decrease in SiO_2 concentration 7between the post-cure and post-gas exposure samples, and leaching of Si from the cement 8was clearly evident from the Si concentration in the product solution over time, which 9increased from <10 to >50 mg/L. These results are reflected in the 57-205 µm deep 10amorphous silica zone identified in the cement cylinders by microanalysis, which is 11indicative of dissolution of the CH and C-S-H in that zone, mobilization of the Ca^{2+} cations, 12followed by re-precipitation of most of the free silica. The CaO content in the pure CO_2 13exposure cement decreased nearly 5 wt% after 84 days, apparently due to leaching of Ca^{2+} 14cations from the cement, as described previously. However, the Ca^{2+} trend in the product 15solution decreased dramatically over time, from >8000 to <2000 mg/L, once CO_2 was 16injected. This apparent contradiction is best explained by calcium carbonate precipitation 17during the CO_2 exposure interval which exceeded the Ca^{2+} dissolution rates. Locally, CH and 18C-S-H had become depleted and replaced by $CaCO_3$, whereby CO_3^{2-} decreased as bicarbonate 19became the dominant aqueous species in the system.

20

21Solids analysis for the cured hydrated cement and post-gas exposure cement samples for the 22CO_2-O_2 gas mixture tests indicated little to no change in SiO_2 and CaO concentration at both 23temperatures (85ºC and 50 ºC). This was reflected by the thinner silica-porous band observed 24in the cement cylinders during microanalysis. While Si concentration in solution increased in 25both the 50ºC and 85ºC tests, these concentrations compare favorably with those observed in 26the pure CO_2 tests, and are thus likely indicative of equilibrium concentrations at the 27experimental parameters utilized. Aqueous Ca^{2+} concentration initially increased after 28 days 28of exposure, from 3400 mg/L to 4400 mg/L in the 50ºC sample, as cations diffused into 29solution, but then decreased in concentration after longer exposure time, likely due to $CaCO_3$ 30precipitation. In contrast, the higher temperature solution displayed a 50% decrease in Ca^{2+} 31concentration after both 28 and 53 days of exposure. These trends suggest that calcium 32carbonate mineral precipitation was favored kinetically at the higher temperature.

33

The free water content in the CO_2-O_2 exposure samples was 7-8 wt % greater than that in the pure-CO_2 samples. However, chemically-bound water content, calculated as the difference between the LOI and other volatiles (CO_2, free moisture, and sulfate) in those same samples was virtually zero, while that in the pure CO_2 samples was 4-7 wt%. This could be interpreted as an indication of the advanced degradation of the cement paste, resulting from the CO_2-O_2 exposure tests, in which all of the hydration water bound in the CH (replaced by $CaCO_3$), ettringite, and C-S-H was freed due to advanced alteration of those phases. The loss of Fe from ferrite grains was not evident based on the solids analysis, as the Fe_2O_3 concentration in the cement pastes was either relatively constant or increased. The increase in Fe, Ni, and Cr concentrations in solution, specifically in the higher temperature sample, suggests that these cations were derived from corrosion of the stainless steel autoclave, which complicates the interpretation of the cement alteration.

Semi-Quantative XRD

Crystalline phase identification of dominant mineral species and precipitated phases post-CO_2 exposure were completed by XRD on the exterior ~2 mm (0.08 in) rim of the cylinders (Table 4). Phases identified in typical hydrated portland cement analysis included portlandite (CH: $Ca(OH)_2$), brownmillerite (C_4AF: $2*Ca_2AlFeO_5$), alite (C_3S: Ca_3SiO_5), belite (C_2S: β-Ca_2SiO_4), a hydrated calcium silicate polymorph pattern (Ca_3SiO_5-type), and an amorphous background hump, indicative of C-S-H. The influence of CO_2 mixed gas exposures on the cements shows the formation of ettringite, hydrotalcite, and carbonates, including calcite, vaterite, aragonite, and trace dolomite.

Carbonation differences were identified between the different gas-exposure samples. The amount of total carbonate is higher in the CO_2-O_2 cement samples than the pure-CO_2 samples. As expected when $CaCO_3$ is a dominate precipitant, CH is low, and vice versa. At both temperatures, the concentration of CH in the CO_2-O_2 tests is significantly lower (50% less) than that in the CO_2 tests. Carbonate formed more rapidly in CO_2-O_2 than pure CO_2, with total $CaCO_3$ nearly double (54.6±3.3 wt%) at elevated temperature, an indication that temperature has a significant influence on carbonation rates as well as C-S-H degradation. The lower temperature sample reflected an increased amorphous content with less carbonation than the higher temperature sample. The addition of oxygen may increase the solubility and efficiency of mineral dissolution in a ligand-type complex behavior. Although calcite was the dominant

carbonate, both vaterite and aragonite appeared to have higher saturation with increasing temperature from 50 to 85ºC.

Precipitation of a hydrotalcite-type (HT) phases is known to occur in hydrated cement, and while only trace amounts were found in pure-CO_2 samples, significant amounts were found throughout all the CO_2-O_2 samples after petrographic and SEM examination. The precipitation of HT is believed to result from hydration coupled either a) with Mg salt attack or b) as an alternative to brucite formation. With a constant supply of Mg-rich brine for hydration, the combination of a less permeable $CaCO_3$ zone and rapid penetration rate of O_2 allowed nucleation of this carbonate only on C_4AF grains, rather than within the C-S-H structure. This released Fe^{3+}, which may have contributed to the cylinder's dark brownish-red, rusty color, more so than seen in the pure-CO_2 exposed samples. The source of Fe was assumed to primarily be the stainless steel autoclave, with only small concentrations derived from C-S-H and ferrite clinker. No siderite, goethite or Fe-oxide were identified by XRD within the cement itself. However, spalled solids collected from the bottom of the vessel did contain goethite and Fe-oxides, which corroborates the presumed source of Fe.

The ettringite increase is of interest because Class H cement has little or no C_3A content; therefore, the main source of Al is from the C_4AF. In the pure-CO_2 samples, sulfur was bound in the C-S-H structure and was fairly uniform in unaltered cement paste. The gypsum (~5 wt %) addition to the cement did not differ in either test as the same cement batch was used. Ettringite was absent in pure CO_2 samples, and increased over time in CO_2-O_2 studies at both exposure temperatures. The ettringite precipitation appeared to be dependent on the rate of CO_2 and O_2 migration into the cement, and occurred after hydrotalcite had formed. As with previous studies examining the Fe-replacement in alumino-ferrite grains, the addition of O_2 must influence the Fe^{2+} present, resulting in ettringite precipitation. This increase, coupled with the formation of microfractures, suggests that detrimental DEF could be initiated at higher temperature exposure.

pH Estimate and Mineral Saturation

The measurement of pH at experimental conditions is difficult but of great interest because carbonic acid produced in a high-pressure CO_2 system is a primary component in the cement reaction sequence. Geochemical modeling of the influence of CO_2 and the CO_2-O_2 mixture was conducted using *CHIM-XPT* methods outlined by Reed and Spycher (24) and Reed (25)

with multiple iterations to demonstrate kinetically-favored phases used to predict mineral saturation and pH at downhole conditions. At selected temperature and pressure conditions *CHIM-XPT* computed the distribution of thermodynamic components of aqueous species, gases, and minerals, using equilibrium constants derived from the database *SOLTHERM*. These equilibrium constants are modifications of mineral thermodynamic data where log K's (saturation index based on dissolution reactions) were computed for cement minerals. The aqueous activity coefficients are determined by using the modified extended Debye-Hückel equation and gas fugacity coefficients (26). A H^+ mass balance was applied to the brine solution chemistry measured at one atmosphere and 25°C to calculate pH under: 1) base pH at neutral waters after the curing process, with a result of 11.8; 2) under CO_2 conditions yielding a pH of 3.0; and 3) CO_2-O_2 mixture conditions with a predicted pH of 3.95. The pH prediction for the solution enhanced the understanding of the pH gradients diffusing into the cement and identified specific conditions for mineral dissolution and precipitation.

The mineral saturation indices were calculated using the post-reacted brine chemical analysis. In both gas exposure experiments, the post-curing interval pH of 11.8 was reflected experimentally by the presence of the CH crystals on the cement cylinder surface, which produced a pH buffer during $CaCO_3$ precipitation. The pure CO_2 solutions were undersaturated in minerals, except for quartz, which was not observed. Modeling of the CO_2-O_2 mixture predicted precipitation of quartz and goethite, which was confirmed experimentally by XRD results of spalled material.

Corrosion of Stainless Steel Autoclaves

The experimental apparatus for the subject tests consisted of stainless steel (316 CrNiMo) autoclave vessels and fittings. Although CO_2 can be corrosive when dissolved in water, carbonic acid has no corrosive impact on stainless steel as confirmed in the pure-CO_2 experiments (27). However, the addition of O_2 led to corrosion due to chloride attack (pitting and/or crevice corrosion), particularly at higher temperature, and termination of the tests after ~ 2 months duration (Fig. 4). The mechanism is too complex for detailed discussion here, but the presence of hydrated iron oxides and lack of $FeCO_3$ in the corrosion products, as identified by XRD, confirms the deleterious role of Cl^- and oxygen in the degradation of stainless steel, which can be explained by the autocatalytic mechanism of pit growth (28).

The CO_2-O_2 gas exposure tests were repeated using Teflon liners placed in the autoclave bodies to prevent further corrosion of the vessel. However, corrosion of the thermocouple thermowell, which extends down into the brine from the autoclave head, led to termination of the repeated tests after 73 days. Lessons learned from the corrosion experienced during these O_2-bearing gas exposure tests include 1) the use of protective liners and/or coatings (Teflon) on all stainless steel parts exposed to the high chloride brine during O_2-bearing gas exposure intervals, 2) curing of the cement cylinder specimens at pressure under argon as a substitute for hydraulic curing, to eliminate the exposure of all fittings in the head to the high chloride brine, and 3) minimization of local static environments created by improper alignment of parts and specimens in the autoclave, which can exacerbate corrosion issues. The corrosion experience and analysis garnered from these tests, while not part of the original test plan, provided valuable insight into the impact of O_2 addition to the gas injection stream. These results suggest that co-sequestration of O_2 may present a significant challenge to the integrity of both the well cement and well casing when injecting the gas mixture into high salinity and higher temperature saline formations.

FURTHER RESEARCH

The effects of co-sequestration using a mixture of ~4% O_2, 1.5% SO_2, and balance CO_2. will also be investigated and compared with the subject tests. The results of these experiments are intended to contribute to the evaluation of co-sequestration as a valid sequestration methodology. Flue gases containing SOx or sour hydrocarbon gas (H_2S) could potentially produce pyrite or other sulfur-bearing species in the cement via mineralization trapping. Additional research on the potential for DEF under these conditions is necessary, as ettringite is a possible precipitate in sulfur gas exposure studies.

CONCLUSIONS

The addition of 4% O_2 to the CO_2 gas injection stream during Class H portland cement exposure tests resulted in rapid formation of $CaCO_3$, enhanced cation diffusion, and mineralogical differences in the cement, compared to pure CO_2 exposure tests. In addition, secondary ettringite formation (possibly DEF), dicalcium silicate (C_2S) polymorphs, and hydrotalcite-like phase were observed in the CO_2-O_2 exposed cements. Modeling of this system suggests that the observed mineralogical changes were made possible by pH changes from the brine into the cement during exposure and extended hydration periods. The formation of delayed ettringite could potentially result in expansion and fracture formation;

however, it is difficult to quantify any direct damage after the duration of subject tests. These observations suggest that the integrity of the wellbore is a concern with O_2 addition to the injected gas stream. Higher salinity and temperature affected the structure of C-S-H and hydration of the cement, which led to higher degradation rate and advanced degradation. Poor cement consolidation, poor bonding to the wellbore casing, or fracture development could lead to corrosion of the casing and degradation of the cement which could provide a leakage pathway along the well bore for the injected gas (CO_2). The potential for corrosion of the steel casing in formations with high chloride brine concentrations was demonstrated, as corrosion of the experimental stainless steel autoclaves was observed in the subject tests.

ACKNOWLEDGMENTS

This work was supported by the Carbon Sequestration Program of the U.S. DOE National Energy Technology Laboratory (NETL). Special thanks to the NETL Seal Integrity team, Barbara Kutchko, Hank Rush, Corinne Disenhof (XRD), James Palandri and Mark Reed (University of Oregon) for contributions. Any opinions or conclusions expressed herein are those of the authors and do not necessarily reflect the views or does not imply endorsement by the United States Department of Energy.

REFERENCES

1. Working Group III of the Intergovernmental Panel on Climate Change, *IPCC Special Report on Carbon Dioxide Capture and Storage*, eds Metz, B., Davidson, O., de Conink, H.C., Meyer, L.A., Cambridge University Press, New York, 2005.
2. Bergman, P.D., and Winter, E.M., *Disposal of Carbon Dioxide in the U.S. Energy Conversion Mgmt*., V. 36, 1995, pp. 523-526.
3. Bruant, R. G.; Guswa, A. J.; Celia, M. A.; and Peters, C. A., "Safe Storage of CO_2 in Deep Saline Aquifers," *Environ. Sci. Technol*., V. 36, 2002, pp. 240-245.
4. Department Of Energy Carbon Sequestration Technology Roadmap and Program Plan, U.S. Department of Energy: Washington, DC, 2007.
5. Carey, J. W.; Wigand, M.; Chipera, S. J.; Wolde Gabriel, G.; Pawar, R.; Lichtner, P. C.; Wehner, S. C.; Raines, M. A.; and Guthrie, G. D., "Analysis and Performance of Oil Well Cement with 30 years of CO_2 Exposure from the SACROC Unit, West Texas, U.S.A.," *Intl. J. Greenhouse Gas Control, V. 1, No.* 1, 2007, pp. 75-85.

16. McGrail, B.P., Schaef, H.T., Ho, A.M., Chien, Y.J., Dooley, J.J., and Davidson, C.L., "Potential for Carbon Dioxide Sequestration in Flood Basalts, *J. of Geophysical Research*, V. 111: B12201, 2006.
47. Mehta and Monteiro. *Concrete: Microstructure, properties, and materials*, 3rd ed., McGraw Hill, 2006.
68. Nelson, E. B., *Well Cementing*. Schlumberger Educational Services, Sugar Land, Texas, 1990.
89. Duguid, A.; Radonjic, M.; and Scherer, G., "Degradation of Well Cements Exposed to Carbonated Brine," *Proceedings of the 4th Annual Conference on Carbon Capture and Sequestration*, May 2-5, 2005, Monitor and Exchange Publications and Forum, Washington D.C.
1210. Hitchon, B., *Aquifer Disposal of Carbon Dioxide*, Sherwood Park, Alberta Resource Council: Geoscience Publishing Ltd, 1996.
1411. Thaulow, N.; Lee, R. J.; Wagner, K.; and Sahu, S., "Effect of Calcium Hhydroxide on the Form, Extent, and Significance of Carbonation," *Calcium Hydroxide in Concrete*; edited by Skalny, J., Gebauer, J., and Odler, I., Eds.; The American Ceramic Society: Westerville, OH, 2001, pp. 191-202.
1812. Kutchko, B. G.; Strazisar, B. R.; Lowry, G. V., Dzombak, and D. A., Thaulow, N., "Rate of CO_2 Attack on Hhydrated Class H Well Cement under Geologic Sequestration Conditions." *Environ. Sci. Technol.*, V. 42, No. 16, 2008, pp. 6237-6242.
2113. Glasser F. P., "The Role of $Ca(OH)_2$ in Portland Cement Concretes," *Calcium Hydroxide in Concrete*, edited by Skalny, J., Gebauer, J., and Odler, I., The American Ceramic Society, Westerville, Ohio, 2001, pp. 11-36.
2414. Pruess, K., and Müller, N., "Formation Dry-Out from CO_2 Injection into Saline Aquifers: 1. Effects of Solids Precipitation and their Mitigation," *Water Resources Research*, V. 45, 2009, W03402, doi:10.1029/2008WR007101.
2715. Zhang, M. and Bachu, S., "Review of Integrity of Existing Wells in Relation to CO_2 Geological Storage: What Do We Know?" *International J. of Greenhouse Gas Control*. V 5, No. 4, 2011, pp. 829-840.
3016. Verba, C.A., O'Connor, W., and Rush, G., "CO_2 Alteration Rates for Class H Portland Cement." *9th Annual Conference on Carbon Capture and Sequestration*, Pittsburgh, PA, U.S.S., May 10-13, 2010.
3317. Crandell, L. E.; Ellis, B. R.; and Peters, C. A., "Dissolution Potential of SO_2 Co-injected with CO_2 in Geologic Sequestration," *Environ. Sci. Technol*., V. 44, 2010, pp. 349-355.

118. Palandri, J.L., and Kharaka, Y.K., “Ferric Iron-Bearing Sediments as a Mineral Trap for CO_2 Sequestration: Iron Reduction using Sulfur-Bearing Waste Gas,” *Chemical Geology*, V. 217, 2005, p. 351-364.
419. Jacquemet, N.; Pironon, J.; and Saint-Marc, J., “Mineralogical Changes of a Well Cement in Various H_2S-CO_2(-brine) Fluids at High Pressure and Temperature,” *Environmental Science & Technology*, 42, 2008, pp. 282-288.
720. Kutchko, B., Strazisar, B., Hawthorn S., Lopano, C., Miller, D., Hakala, A., and Guthrie, G. “H_2S-CO_2 Reaction with Hydrated Class H Well Cement: Acid-Gas Injection and CO_2 Co-sequestration,” *Environmental Science and Technology*. V. 5, No. 4, 2011, pp. 880-888.
1121. API. Recommended Practice for Testing Well Cements; *API Recommended Practice 10B*; API: Washington, DC, 1997; pp. 133.
1322. NATCARB, NatCarb: 2008, <http://www.natcarb.org>.
1423. International Centre for Diffraction Data, Powder Diffraction File Update, 2008, PDF-2.
1524. Reed, M.H., and Spycher, N.F., “Calculation of pH and Mineral Equilibria in Hydrothermal Water with Application to Geothermometry and Studies of Boiling and Dilution,” *Geochim. Cosmochim. Acta*, V. 48, 1984, pp. 1479-1490.
1825. Reed, M.H., “Techniques in Hydrothermal Ore Deposits Geology,” Chapter 5, *Reviews in Economic Geology*, V. 10, 1998, pp. 109-124.
2026. Tanger IV, J.C., and Helgeson, H.C., “Calculation of the Thermodynamic and Transport Properties of Aqueous Species at High Temperatures and Pressures: Revised Equations of State for the Standard and Partial Molal Quantities of Ions and Electrolytes,” *Am. J. Sci.* V. 288, 1988, pp.19– 98.
2427. *Corrosion Resistance of the Austenitic Chromium-Nickel Stainless Steels in Chemical Environments*, International Nickel Company, Inc., 1963.
2628. Ziomek-Moroz, M., O’Connor, W., and Bullard, S., *Investigations of Localized Corrosion of Stainless Steel after Exposure to Supercritical CO_2*, National Association of Corrosion Engineers (NACE) Corrosion 2012 Conference, March 2012.

TABLES AND FIGURES

Table 1-- Total alteration depth of CO_2 and CO_2-O_2 exposure at 50/85°C. Alteration depth of CO_2 from Verba, 2011.

Gas Type	Temperature (°C)	Exposure Duration	Alteration depth (µm)
CO_2	50	28	151±20
CO_2	50	56	714±61
CO_2	50	84	1254±441
CO_2-O_2	85	28	253±59
CO_2-O_2	85	53	737±94
CO_2-O_2	85	73	1585±422
CO_2-O_2	50	28	514±109
CO_2-O_2	50	56	680±132
CO_2-O_2	50	73	700±100

Table 2-- Solid chemical compositions of the unhydrated cement, the cured hydrated cement paste, and cement paste post-CO_2 and CO_2-O_2 exposure (wt%). Unit conversion: 100 µm = 0.003937 in

Oxide wt%	Cement Powder	Cured Paste	CO_2 50°C	CO_2-O_2 50°C	CO_2-O_2 85°C
SiO_2	21.07	17.95	17.02	18.39	17.99
Al_2O_3	2.78	2.4	2.26	2.3	2.33
Fe_2O_3	4.37	3.64	3.54	5.64	3.77
CaO	64.02	54.55	49.82	52.25	52.45
MgO	2.94	2.49	2.27	2.39	2.29
Na_2O	0.05	0.09	<0.01	<0.01	0.01
K_2O	0.11	0.1	0.01	0.01	0.02
Cr_2O_3	0.01	0.01	0.02	0.02	<0.01
TiO_2	0.2	0.17	0.18	0.15	0.16
MnO	0.06	0.05	0.05	0.07	0.07
P_2O_5	0.131	0.113	0.105	0.107	0.116
SrO	0.1	0.08	0.06	0.08	0.08
BaO	0.07	0.05	0.04	0.05	0.06
LOI[1]	0.73	16.85	22.9	17.05	18.9
Total	96.64	98.55	98.27	98.5	98.25
C	0.07	1.65	2.35	1.14	0.9
CO_2	0.3	6.1	8.6	3.5	3.2
FeO	0.19	0.19	0.13	0.26	0.19
H_2O [2]	<0.01	5.55	4.93	11.9	13.7
S	0.17	0.06	0.17	0.11	0.17
SO_3 [3]	2.48	2	1.8	1.93	1.68

[1] LOI: Loss on Ignition, measured as the weight loss after 1 hour at 1000 C, in air.

[2] Free moisture, measured as the weight loss after 1 hour at 105 C, in air.

[3] Sulfate sulfur- carbonate leach

Table 3-- Brine solution chemical compositions of the post-cured solution and the post-gas exposure solutions taken at several exposure intervals (mg/L).

(mg/L)	Surrogate CO_2 50°C				Surrogate CO_2-O_2 50°C				Surrogate CO_2-O_2 85°C		
	Cured	Exposure			Cured	Exposure			Cured	Exposure	
Duration (days)	28	28	56	84	28	28	56	66	28	28	53
HCO_3	*	*	*	*	665	945	335	287	335	451	402
Cl-	40700	37300	38100	39700	28000	31000	33000	17000	28000	31000	28000
SO4 2-	<1	8	7	8	480	50	100	100	1200	100 [1]	100 [1]
Ca	8450	1869	1770	1694	3400	4400	3800	3600	4100	2000	2100
Cr	0.0226	0.033	<DL	<DL	1.4	5.8	3.3	28	0.7	8.5	0.5 [1]
Fe	0.0196	0.167	0.549	0.263	5	36	20	200	5	66	5 [1]
K	6.13	59.8	56.6	57	750	79	120	110	600	50 [1]	62
Mg	626	1395	948	784	79	360	430	660	50	360	350
Na	24160	25530	18200	19700	14000	16000	17000	21000	13000	17000	14000
Ni	1 [1]	12.58	15.85	22.94	1	61	180	380	1 [1]	750	260
Si	7.644	47.6	53.68	52.01	5.1	51	51	46	2.5 [1]	78	9
Free CO_2	*	*	*	*	5.10E-05	1300	62	46	1.0E-04	950	17

[1] concentration at or below detection limit

* no measurement

Table 4-- XRD analyses of CO_2 and CO_2-O_2 exposure comparing the semi-quantified concentrations of minerals present due to gas and temperature differences in weight percent.

	Pure CO_2 50°C	96% CO_2-4% O_2 85°C		96% CO_2-4% O_2 50°C	
	84 days	28 days	53 days	28 days	56 days
Portlandite $Ca(OH)_2$	24.2±4.2	10.5±1.8	11.2±2.1	19.5±1.2	12±2.1
Brownmillerite Ca_2FeAlO_5	8.8±1.5	8.3±1.2	8.3±1.8	12.4±1.8	5.3±0.9
Hatrurite Calcium Silicate Ca_3SiO_5	17±2.1	6.3±1.2	13.8±3.9	12.1±2.1	10±2.4
Larnite $Ca_2(SiO_4)$	16.6±4.8	13.4±3.9	13.5±3.9	9.5+0.3	2.7±1.5
Ettringite $Ca_6(Al(OH)_6)_2(SO_4)_3(H_2O)_{25.7}$	0	3.9±0.9	7.5±2.1	9.6±2.1	12±2.4
Hydrotalcite $Mg_6Al_2(CO_3)(OH)_{16}*4H_2O$	trace	2.3±0.9	2.3±1.2	4.2±1.2	3.5±0.9
Total $CaCO_3$ (Calcite, Vaterite, Aragonite)	22.5±3.9	54.6±3.3	54.2±1.9	26.7±1.2	23.2±2
Amorphous	1.9±0.9	0.6±0.3	2.2±4.2	6±0.3	30.7±4.2

Error = reported error x3, Materials Data Inc., Jade

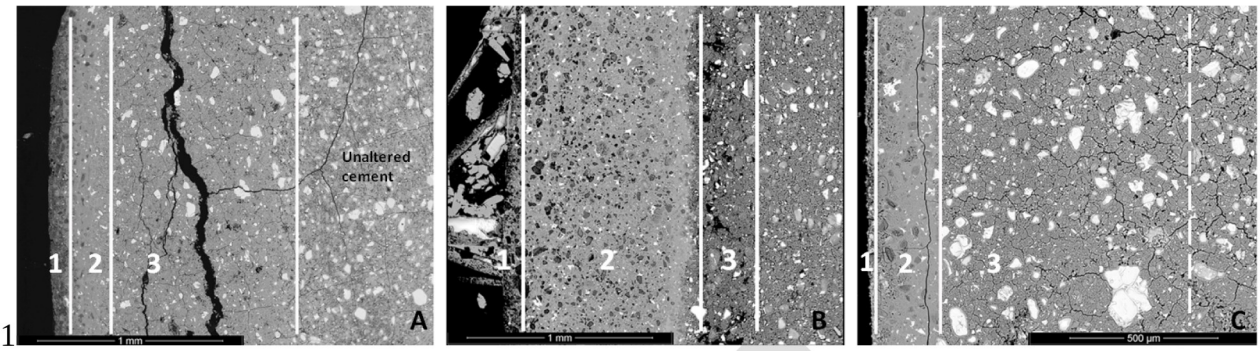

Fig. 1-- Carbonation and alteration depth of portland cement cylinders exposed to A) 84 days and pure-CO_2 at 50ºC, B) 53 days CO_2-O_2: 85ºC, and C) 66 days CO_2-O_2 50ºC. Zone 1 is the porous-Si, zone 2 is $CaCO_3$, and zone 3 is the Ca^{2+} leading into unaltered cement. Dashed line indicates diffuse Ca^{2+} leached zone; no boundary. Scale bar 1 mm (0.04 in).

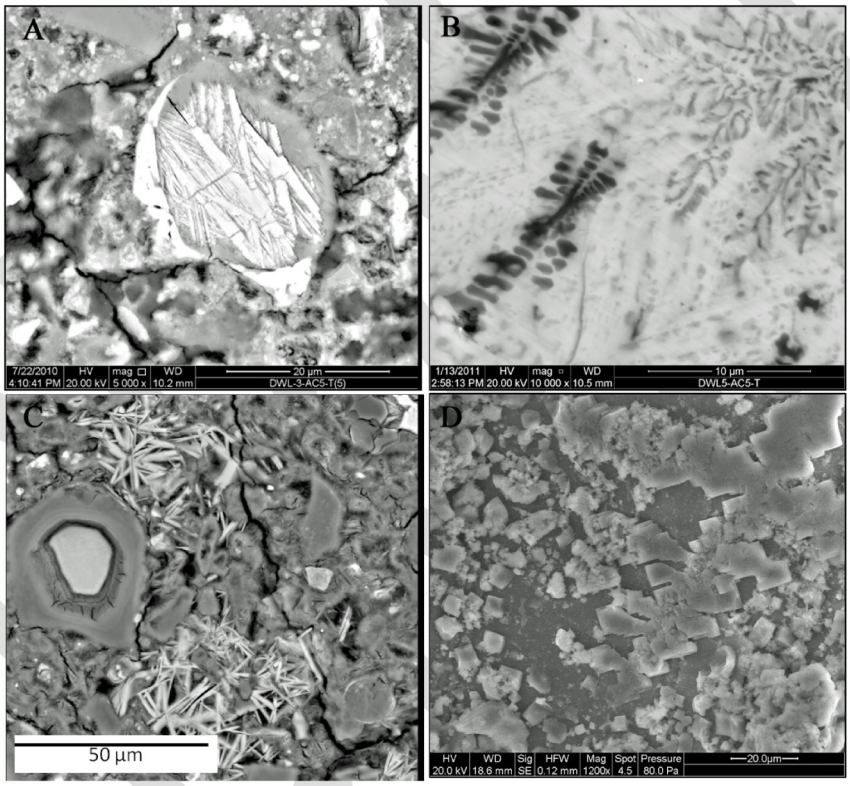

Fig. 2-- Minerals and polymorphs in CO_2-O_2 injected samples. A) Calcium silicate polymorph, B) Hydrotalcite forming on ferrite grains, C) Ettringite needles in the Ca^{2+} depleted zone, and D) Cubic halite grains within the carbonated zone.

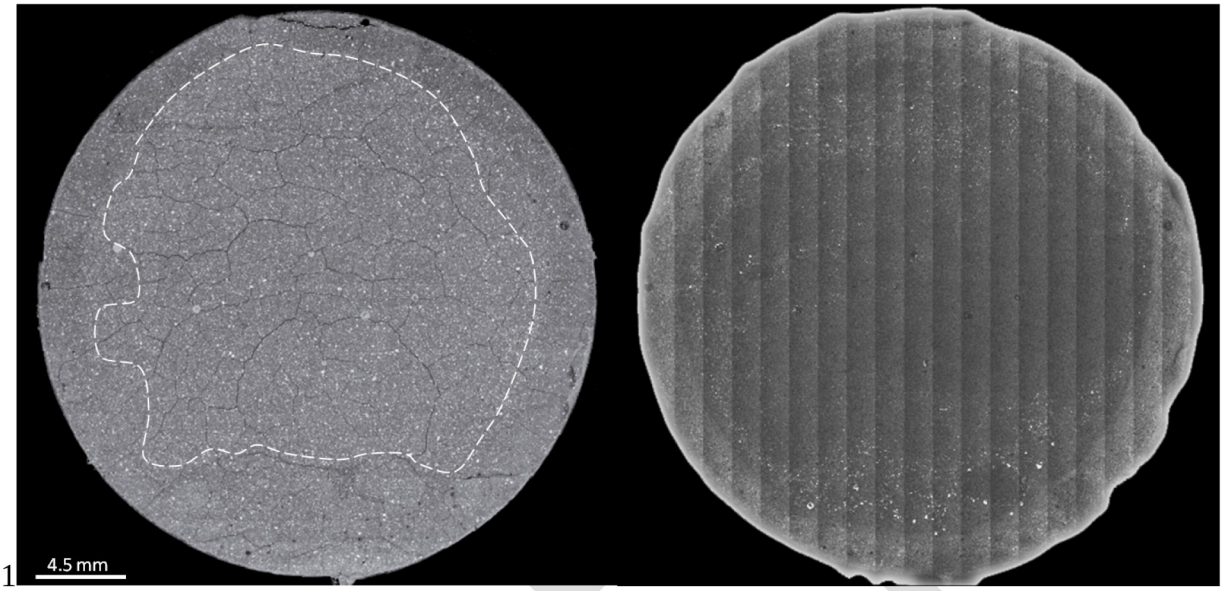

Fig. 3-- Montage backscatter (BSE) image (left) and Ca^{2+} EDS map (right) of CO_2-O_2 exposure sample with diffuse alteration boundary (white outline) extending into the cylinder. Scale 4.5 mm (0.18 in)

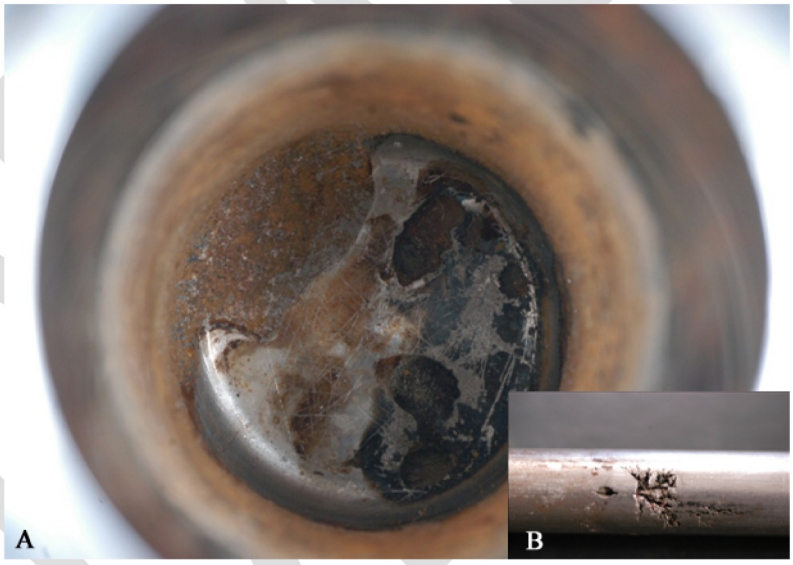

Fig. 4-- A) Chloride attack on stainless steel autoclave and B) thermocouple thermowell corrosion result of CO_2-O_2 exposure tests.